Journal of Electron Spectroscopy and Related Phenomena 196 (2014) 80–84

Contents lists available at ScienceDirect

Journal of Electron Spectroscopy and Related Phenomena

journal homepage: www.elsevier.com/locate/elspec

X-ray phase-contrast CT imaging of the acupoints based on synchrotron radiation

Liu Chenglin [a,*], Wang Xiaohua [a], Xu Hua [a], Liu Fang [b], Dang Ruishan [b], Zhang Dongming [c], Zhang Xinyi [c], Xie Honglan [d], Xiao Tiqiao [d]

[a] Physics Department of Yancheng Teachers' College, Yancheng 224051, China
[b] Anatomy Department of Second Military Medical University, Shanghai 200433, China
[c] Synchrotron Radiation Research Center of Fudan University, Shanghai 200433, China
[d] Shanghai Synchrotron Radiation Facility of Shanghai Institute of Applied Physics, CAS, Shanghai 201800, China

ARTICLE INFO

Article history:
Available online 30 December 2013

Keywords:
Acupoints
Morphology
In-line phase-contrast
CT imaging
Synchrotron radiation

ABSTRACT

In this paper, the morphology of the acupuncture point (abbreviated as acupoint hereafter) or tissue where there were no acupoints in the fractional rabbit hind limb was studied by in-line phase contrast CT imaging (PCI-CT) methods based on synchrotron radiation. The density of micro-vessels was calculated for tissues with acupoints or without acupoints. Differences between acupoints area and non-acupoint areas determined by the density of the micro-vessels propose a strong evidence of the existence of acupoints. Our results showed that there were two significantly higher densities of the micro-vessels, where two acupoints were located, respectively. In addition, there were large numbers of involutedly microvascular structure in the acupoint areas. Nevertheless, in non-acupoints area, the microvascular structure was relatively simple and flat.

1. Introduction

The meridian theory is one of the most important concepts of the Chinese Medicine theory. Through continually practice and validation for thousands years, the meridian theory and acupuncture technology have been spread so far, and been commonly used in the medical profession today. However, the meridian theory is summarized from a large number of human clinical experience, some are still speculative conclusions and lack of experimental demonstration due to its complexity. Hence, there will be great biological significance and clinical value to clarify and reveal the essence of the meridians, acupoints, and the mechanism of acupuncture [1,2].

The meridian essences have been explored since ancient times and continuously investigated with the development of science and technology in recent years. It is well known that in one meridian some specific acupoints locate. A lot of theories and the hypotheses about meridian have been proposed, such as the nerve theory, nerve-endocrine theory, neurovascular theory, and connective tissue theory [3,4]. The research methods mainly consist of the magnetic resonance imaging (MRI), anatomy, computed tomography (CT), infrared imaging, LCD thermal photography method, and ultrasonic photography method [5–7]. Many studies have shown that each meridian has of their own unique characteristics. At the same time, these results show that the acupoints are existed.

In recent years, owing to the high brightness, wide spectrum, high collimation, polarization, and pulsed structure of synchrotron radiation [8,9], it has been vastly applying in various researches, such as physics, chemistry, life sciences, medicine, materials science, and geological sciences. In addition, there are extremely important applications in industry [10].

When the X-rays pass through the object, their amplitude and their phase would be changed. In the conventional X-ray imaging, only the contrast resulted from the changes of amplitude will be recorded, but the soft tissue is almost transparent to hard X-rays, and the amplitude contrast (or say, absorption contrast) cannot clearly reveal the internal information of the object. As we know, the phase shift is determined by the real part of a refraction index. It is about 1000 times bigger than its imaginary part, which results in the change of absorption of X-rays pass through objects. Therefore, to record the phase shift is more sensitive than the change of absorption. The former is called the phase contrast. This is the mechanism of the X-ray phase contrast imaging (XPCI), which has been quickly developed to form the X-ray phase contrast CT imaging (XPCT) after the combination of XPCI and the computed tomography (CT). In recent years, several XPCT methods have been proposed, such as in-line X-ray phase contrast CT (IL-XPCT)

* Corresponding author. Tel.: +86 51588233178; fax: +86 51588233179.
E-mail addresses: lclyctc@163.com, lclyctu@163.com (L. Chenglin).

0368-2048/$ – see front matter © 2013 Elsevier B.V. All rights reserved.
http://dx.doi.org/10.1016/j.elspec.2013.12.005

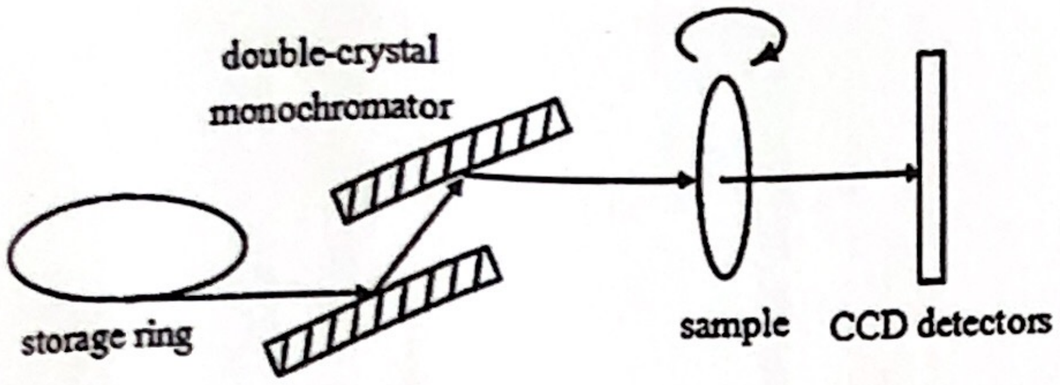

Fig. 1. X-ray micro-CT imaging schematic diagram.

and diffraction enhanced CT imaging (DEI CT) [11–15]. The in-line X-ray phase contrast CT method has been mainly used by many researchers due to its simplicity [16–18]. The small changes of density or contours can be easily found by in-line imaging technology because there is a certain space coherent for the synchrotron radiation. In-line imaging technology is also a direct imaging through the enhanced edge effect of the sample and without the need for phase recovery. Relative to the other phase contrast imaging methods, the in-line imaging has some advantages, such as simple light path, large view field, image intuitive, and without artifacts. It is also suitable for microscopy imaging or CT imaging. There is a very simple principle for the combination of microscopy imaging and computed tomography, i.e. microscopy tomography (μ-CT), which is similar to the well-known medical CT [19]. When the μ-CT is used in object imaging, a series of projected images (typically 1000 or more) are recorded by CCD or films when the sample is rotated in 0–180° angle around an axis perpendicular to the photon beam. These images are then reconstructed and formed a three-dimensional (3D) image of original object by CT software.

2. Experimental method and sample

2.1. Experimental setup and imaging method

Experiments were carried out at the X-ray beam imaging and biomedical applications station, BL13W1, at Shanghai Synchrotron Radiation Facility. The electron energy in storage ring is 3.5 GeV, the beam intensity is about 100–210 mA, and the photon energy is in the range of 8–72.5 keV. Fig. 1 is the experimental setup of phase contrast CT imaging [20]. During experiments, a monochromatic light was adjusted at the energy of 21 keV, the light spot had a size of 18.9 mm × 5.5 mm on the sample, and the recorded image size was 2100 × 631 pixels, approximately. The sample was fixed in a rotating stage, the images were recorded by an imaging detector CCD (Photonic-science Ltd., UK) with 9 μm effective pixel size, the detector was adjusted at 0.5 m away from the sample, and the exposure time was about 5 ms for all images. The basic experimental procedure included three steps: recording the projections of the sample (XPCIs), collecting slices images from all XPCIs, and reconstructing the three-dimensional image (please see Fig. 2 of Ref. [19]). In recording the projection of the sample, the sample is divided into six segments along the *z*-axis direction and continuously imaged as shown in Fig. 2, and every segment is about 6.615 mm in height. In imaging, the sample stage was rotated by 180° around *z*-axis with a speed of 0.2°/s for CT scanning.

2.2. Sample preparation

Ten samples were provided by the Department of Anatomy, the Second Military Medical University. These samples were taken from adult white New Zealand rabbits. The rabbit was anesthetized using large doses of anesthetic, and then injected 5% sodium citrate to anticoagulant blood vessels from abdominal aorta in order to outflow blood and clear the blood-vessels. Then, the contrast agent, a mixture solution including barium sulfate and emulsion (particle diameter is about a few hundred nanometers), was injected into the blood vessels from abdominal aorta, so that the alignment and morphology of the vessels were more clearly in image of the sample. About 15 min later, the required samples were removed from the rabbit, and then they were soaked and fixed in a solution of formalin.

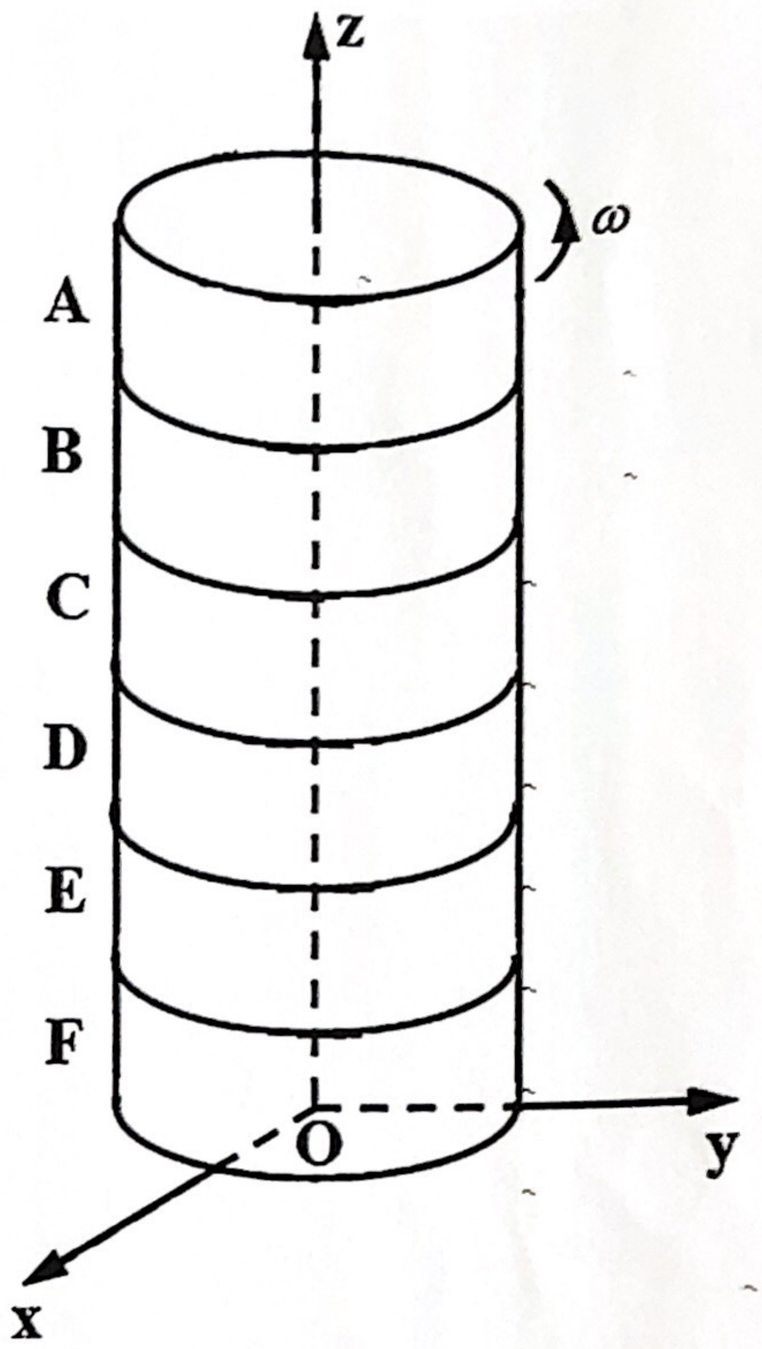

Fig. 2. The schematic diagram of the samples.

The experimental sample was the muscle tissue selected from outside the hind limb of the rabbit, and had a shape of cylinder with a height of 39.69 mm and a diameter of 11.34 mm approximately. There are two acupoints, Housanli acupoint (Zusanli in the human body, ST36) (at B in Fig. 3) and Shangjuxu acupoint (ST37) (at E in Fig. 3) in the sample according to the literatures [21–24]. Fig. 3 is a picture of the sample, the letter B represents the Housanli acupoint, the letter E represents the Shangjuxu acupoint, and letters A, C, D and F refer to the area of no acupoints, respectively.

3. Results and discussion

3.1. The structure image of the acupoints along meridian direction

Fig. 4 is one of the XPCI projection images of the sample. The Housanli acupoint and Shangjuxu acupoint are located at areas B and E, respectively, and the other parts are no acupoint areas. The circled areas are acupoint areas, as shown in Fig. 4. The areas B and E are not on a line and thus these two points are in different meridians. The structure of the area E is very clear but the area B is not, which implies that these two points are not in same depth.

Fig. 3. The photo of the samples.

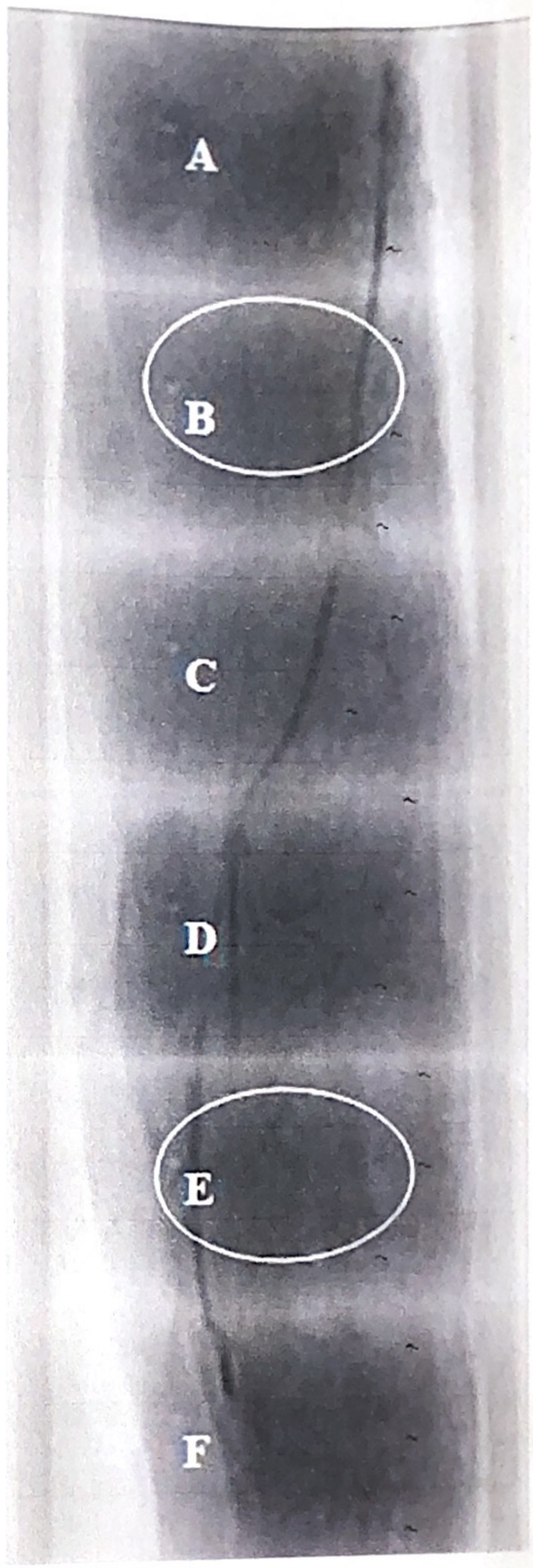

Fig. 4. The XPCI projection image of the sample.

In acupoint's areas, the small microvascular and their bifurcation can be clearly seen around the thick blood vessels, but only few thick blood vasculars with no fine structures can be seen in non-acupoint areas. In addition, these images are only two-dimensional ones in the projection plane of the three-dimensional structure of the sample, which should be the duplication of internal structure of the sample.

3.2. The structure image of the acupoints perpendicular to meridian direction

Fig. 5 shows the tomographic slices of the sample, which are images made by using a large number of projection images of the sample; they are the structural images of the acupoints perpendicular to the meridian direction. The three-dimensional structure of the acupoints can be reconstructed based on these slices (Fig. 5). The tomographic slices show that the X-ray absorption coefficient is different for the muscle tissue of different areas in the sample. It will result in a contrast difference between different organizations. The most direct result is the change of dark or bright in different areas. Comparing these tomographic slices, it is possible to see that there are different diameters and distributions of the blood vessels in various slices. In the acupoint areas, there are relatively small diameters for the microvascular, which are relatively dense (i.e. aggregation), but the vasculars are relatively few and dispersive in non-acupoint regions.

3.3. The quantitative results of micro-vascular aggregation

For expressing quantitatively the micro-vascular aggregation in acupoint regions, the relative distribution of vascular areas (Aa%) and the relative average gray degree (Gg%) of blood vessels were calculated using an image analysis software [25]. The relative vascular distribution Aa% is defined as the ratio of blood vessel area to the acupoint areas, and the relative average gray degree Gg% is the ratio of the average gray degree of the blood vessels region to the average gray degree of acupoint areas. The vascular density (AaGg%) is the products of Aa% and Gg% of the vascular [26]. The calculation results are shown in Table 1 and Fig. 6. It can be clearly seen that the vascular density (AaGg%) is higher in the acupoints than that in the non-acupoint area, hence there is a micro-vascular aggregation in the acupoint areas. At the same time, the relative distribution of the vascular area is significantly increased in the acupoint region, and the periodic variation is shown in Fig. 6. The distance between the centers of the areas B and E is consistent with the results in the theory of Chinese Medicine. These may

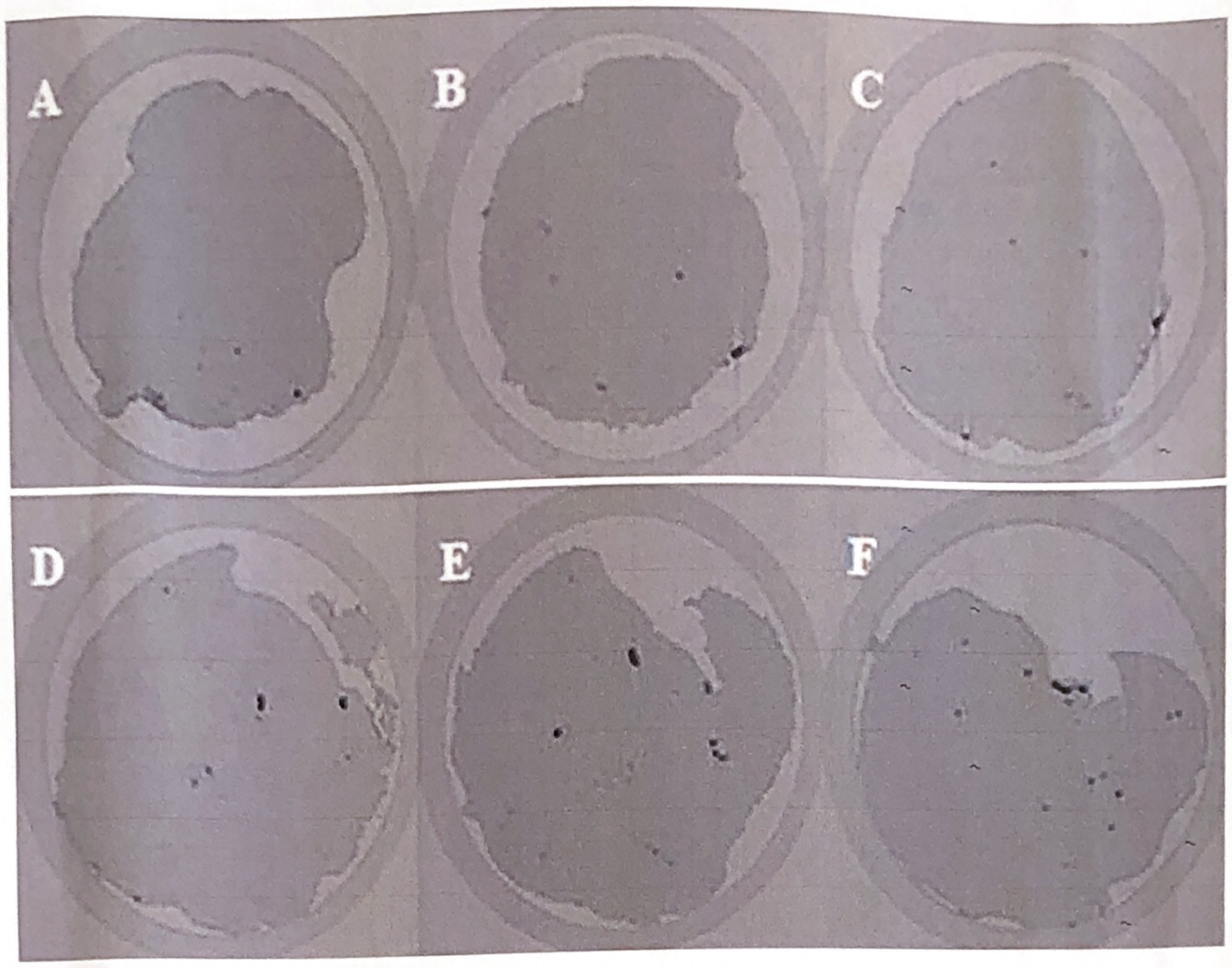

Fig. 5. The structural image of the acupoints perpendicular to meridian direction.

Table 1
Aa%, Gg% and AaGg% values of the sample.

Area	The relative area of the vascular (Aa%)	The relative average gray (Gg%)	AaGg%	Remark (is acupressure point?)
A	8.97 ± 2.81	19.24 ± 0.24	172.51 ± 54.04	No
B	8.33 ± 2.25	67.16 ± 0.06	559.38 ± 151.39	Yes
C	10.43 ± 2.59	30.13 ± 0.12	314.43 ± 77.90	No
D	13.76 ± 4.27	17.13 ± 0.04	235.64 ± 73.21	No
E	10.53 ± 1.33	75.06 ± 2.88	790.41 ± 99.46	Yes
F	18.22 ± 8.06	10.68 ± 0.26	194.69 ± 86.13	No

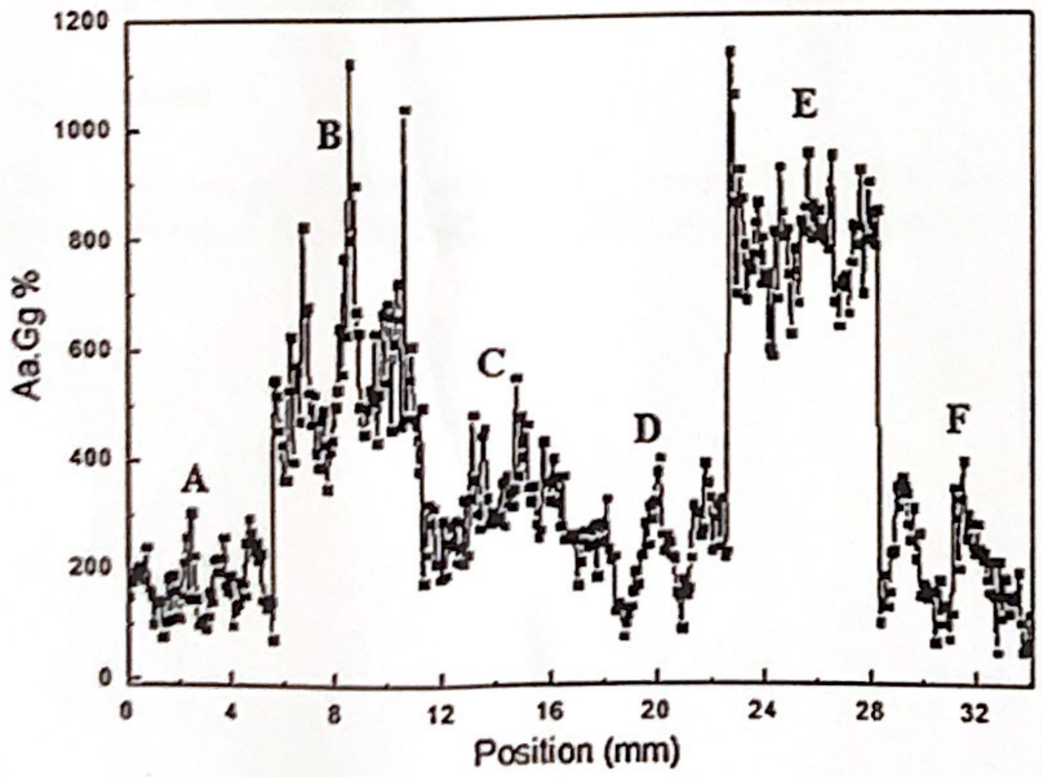

Fig. 6. The calculation results of the vascular density.

reflect a bifurcation phenomenon for the micro-vascular in acupoint regions.

3.4. 3D reconstructed image of the phase contrast CT

Fig. 7 is the 3D reconstructed image of the entire sample by IL-XPCT, which includes two acupoints and non-acupoint areas with a spatial resolution of about 18 μm. The area B is Housanli acupoint, the area E is Shangjuxu acupoint, and others (A, C, D, F) are non-acupoint areas, as shown in Fig. 7. In these 3D images, some microstructures can be observed, such as some large vessels with many fine branching vasculars in area B or E. The largest one is approximately 50 μm in diameter in these vasculars, which are small arteries. The fine branch vessels, with the diameter in the range of 15–40 μm, are small veins or micro-vessels. However, a small amount of thick blood with almost no micro-structure can be observed in non-acupoint areas (A, C, D, F). In the acupoints, there are some aggregations of the microvasculars with a diameter of about dozens of microns, but this characteristic is not obvious in non-acupoint areas.

Fig. 7. Three-dimensional reconstructed image of the sample.

4. Conclusions

The morphology of the acupoints was studied using the synchrotron-based IL-XPCT method. From the three dimensional images, it is easy to find the microvascular aggregations in the acupoint areas. The size of an acupoint can be estimated by the diameter of microvascular aggregations, which is about 5 mm for rabbit. It is consistent with our previous results determined by the size of trace elements-rich area [27]. Our results demonstrated again the existence of acupoints, and also show that the acupoints are special points in mammals.

Acknowledgements

This work was supported by the National Natural Science Foundation of China (Grant No. 11175152). We also would like to thank the staffs at SSRF BL13W for their technical support in IL-XPCT experiments.

References

[1] X.H. Yan, X.Y. Zhang, et al., Phys. Med. Biol. 54 (2009) N143–N150.
[2] Y. Zhang, X.H. Yan, C.L. Liu, et al., J. Lumin. 119–120 (2006) 96–99.
[3] J.J. Tsuei, IEEE Eng. Med. Biol. Mag. 15 (3) (1996) 58–63.
[4] L. Li, T. Yau, C.-H. Yau, J. Acupunct. Tuina Sci. 10 (2) (2012) 125–127.
[5] X.J. Song, D. Zhang, Chin. Acupunct. Moxibustion 30 (1) (2010) 51–54 (in Chinese).
[6] P. Liu, G.Y. Zhou, Y. Zhang, et al., Neurosci. Lett. 479 (2010) 267–271.
[7] L. Fei, H.S. Cheng, et al., Chin. Sci. Bull. 439 (6) (1998) 658–672 (in Chinese).
[8] C.Z. Yang, G.F. Cheng, Y.H. Huang, Phys. Test. Chem. Anal. Part A: Phys. Test. 44 (2) (2008) 103–106 (in Chinese).
[9] A.A. Zholents, M.S. Zolotorev, Phys. Rev. Lett. 76 (6) (1996) 912–915.
[10] R. Lewis, Phys. Med. Biol. 42 (1997) 1213–1243.
[11] R.C. Chen, D. Dreossi, L. Mancini, et al., J. Synchrotron Radiat. 19 (5) (2012) 836–845.
[12] F.A. Dilmanian, Z. Zhong, B. Ren, et al., Phys. Med. Biol. 45 (4) (2000) 933–946.
[13] Z.F. Huang, K.J. Kang, Z. Li, et al., Appl. Phys. Lett. 89 (2006) 041124.
[14] P.P. Zhu, J.Y. Wang, Q.X. Yuan, et al., Appl. Phys. Lett. 87 (2005) 264101.
[15] C.L. Liu, X.H. Yan, X.Y. Zhang, et al., Phys. Med. Biol. 52 (2007) 419–427.
[16] A.V. Bronnikov, J. Opt. Soc. Am. A 19 (3) (2002) 472–480.
[17] H.L. Xie, B. Deng, G.H. Du, et al., Mod. Phys. 3 (2010) 42–50.
[18] P. Spanne, C. Raven, I. Snigireva, Phys. Med. Biol. 44 (3) (1999) 741–749.
[19] D.M. Zhang, X.H. Yan, X.Y. Zhang, et al., Anal. Bioanal. Chem. 401 (3) (2011) 803–808.
[20] C.L. Liu, H. Xu, C.Y. Chen, IEEE BMEI 2011 1 (2011) 572–574.
[21] L.Y. Zheng, Z.X. Xu, X.C. Zhen, et al., Shanghai J. Acu-Mox. 22 (5) (2003) 26–29 (in Chinese).
[22] Q. Shu, Y. Xu, H. Yang, et al., Shanghai J. Anim. Husbandry Vet. Med. 1 (1982) 17–23 (in Chinese).
[23] Q. Shu, Y. Xu, H. Yang, et al., Shanghai J. Anim. Husbandry Vet. Med. 2 (1982) 10–13 (in Chinese).
[24] Q.S. Ren, X.Q. Chen, J.L. Wang, et al., Chin. J. Surg. Integr. Tradit. West. Med. 17 (6) (2011) 586–589 (in Chinese).
[25] C.J. Gao, E.Y. Chen, G.J. Cai, Anat. Clin. 10 (2) (2005) 98–100.
[26] W.F. Lu, Z.H. Dong, Z.J. Liu, et al., J. Surg. Res. 164 (1) (2010) e193–e199.
[27] X.H. Yan, X.Y. Zhang, C.L. Liu, et al., J. Phys.: Conf. Ser. 186 (2009) 012100.